AFRL-AFOSR-VA-TR-2016-0281

MANIPULATING THE INTERFACIAL ELECTRIAL & OPTICAL PROPERTIES OF DISSIMILA

Seth Bank
UNIVERSITY OF TEXAS AT AUSTIN
101 EAST 27TH STREET STE 4308
AUSTIN, TX 78712

08/03/2016
Final Report

Air Force Research Laboratory
AF Office Of Scientific Research (AFOSR)/RTA1

Arlington, Virginia 22203
Air Force Materiel Command

REPORT DOCUMENTATION PAGE

Form Approved
OMB No. 0704-0188

PLEASE DO NOT RETURN YOUR FORM TO THE ABOVE ORGANIZATION.

1. REPORT DATE *(DD-MM-YYYY)*	2. REPORT TYPE	3. DATES COVERED *(From - To)*
30-07-2016	Final	1 May 2010 - 30 Apr 2016

4. TITLE AND SUBTITLE

Manipulating the Interfacial Electrical & Optical Properties of Dissimilar Materials with Metallic Nanostructures

5a. CONTRACT NUMBER

FA9550-10-1-0182

5b. GRANT NUMBER

5c. PROGRAM ELEMENT NUMBER

6. AUTHOR(S)

Seth R. Bank

5d. PROJECT NUMBER

5e. TASK NUMBER

5f. WORK UNIT NUMBER

7. PERFORMING ORGANIZATION NAME(S) AND ADDRESS(ES)

The University of Texas at Austin
101 E. 27th, Ste 4308
Austin, TX 78712-1500

8. PERFORMING ORGANIZATION REPORT NUMBER

9. SPONSORING/MONITORING AGENCY NAME(S) AND ADDRESS(ES)

Air Force Office of Scientific Research
875 North Randolph Street, Rm 3112
Arlington, VA 22203

10. SPONSOR/MONITOR'S ACRONYM(S)

AFOSR

11. SPONSOR/MONITOR'S REPORT NUMBER(S)

12. DISTRIBUTION/AVAILABILITY STATEMENT

UU (Unclassified Unlimited)

13. SUPPLEMENTARY NOTES

N/A

14. ABSTRACT

The future of AF sensing is multi-modal imaging sensors that vertically integrate an ever increasing diversity of modes (wavelength bands, polarization states, phase, etc.) onto each pixel. A fundamental challenge is manipulating the electrical and optical properties at the interface of dissimilar materials. We sought to address the traditional challenges associated with this need via the integration of precisely controlled (semi) metallic nanostructures with III-V semiconductors, using ErAs and related materials as the metals. Our approach began with coupling these metallic nanostructures with growth on patterned templates. We developed a patterning/regrowth process and characterized the deposition of ErAs on a variety of template surfaces using a variety of electrical, optical, structural, and chemically-sensitive techniques. We also examined the optical quality of III-V layers grown above ErAs nanostructures, which is critical for future device applications, and developed a method to achieve optical quality within 80-95% of nominally-identical Er-free structures. These findings led us to invent a technique to grow GaAs that is free of planar

15. SUBJECT TERMS

Molecular Beam Epitaxy, Nanostructures, Multimodal Sensors

16. SECURITY CLASSIFICATION OF:			17. LIMITATION OF ABSTRACT	18. NUMBER OF PAGES	19a. NAME OF RESPONSIBLE PERSON
a. REPORT	b. ABSTRACT	c. THIS PAGE			Seth R. Bank
UU	UU	UU	N/A	17	19b. TELEPHONE NUMBER *(Include area code)* 512-471-9669

Reset

INSTRUCTIONS FOR COMPLETING SF 298

1. REPORT DATE. Full publication date, including day, month, if available. Must cite at least the year and be Year 2000 compliant, e.g. 30-06-1998; xx-06-1998; xx-xx-1998.

2. REPORT TYPE. State the type of report, such as final, technical, interim, memorandum, master's thesis, progress, quarterly, research, special, group study, etc.

3. DATES COVERED. Indicate the time during which the work was performed and the report was written, e.g., Jun 1997 - Jun 1998; 1-10 Jun 1996; May - Nov 1998; Nov 1998.

4. TITLE. Enter title and subtitle with volume number and part number, if applicable. On classified documents, enter the title classification in parentheses.

5a. CONTRACT NUMBER. Enter all contract numbers as they appear in the report, e.g. F33615-86-C-5169.

5b. GRANT NUMBER. Enter all grant numbers as they appear in the report, e.g. AFOSR-82-1234.

5c. PROGRAM ELEMENT NUMBER. Enter all program element numbers as they appear in the report, e.g. 61101A.

5d. PROJECT NUMBER. Enter all project numbers as they appear in the report, e.g. 1F665702D1257; ILIR.

5e. TASK NUMBER. Enter all task numbers as they appear in the report, e.g. 05; RF0330201; T4112.

5f. WORK UNIT NUMBER. Enter all work unit numbers as they appear in the report, e.g. 001; AFAPL30480105.

6. AUTHOR(S). Enter name(s) of person(s) responsible for writing the report, performing the research, or credited with the content of the report. The form of entry is the last name, first name, middle initial, and additional qualifiers separated by commas, e.g. Smith, Richard, J, Jr.

7. PERFORMING ORGANIZATION NAME(S) AND ADDRESS(ES). Self-explanatory.

8. PERFORMING ORGANIZATION REPORT NUMBER. Enter all unique alphanumeric report numbers assigned by the performing organization, e.g. BRL-1234; AFWL-TR-85-4017-Vol-21-PT-2.

9. SPONSORING/MONITORING AGENCY NAME(S) AND ADDRESS(ES). Enter the name and address of the organization(s) financially responsible for and monitoring the work.

10. SPONSOR/MONITOR'S ACRONYM(S). Enter, if available, e.g. BRL, ARDEC, NADC.

11. SPONSOR/MONITOR'S REPORT NUMBER(S). Enter report number as assigned by the sponsoring/ monitoring agency, if available, e.g. BRL-TR-829; -215.

12. DISTRIBUTION/AVAILABILITY STATEMENT. Use agency-mandated availability statements to indicate the public availability or distribution limitations of the report. If additional limitations/ restrictions or special markings are indicated, follow agency authorization procedures, e.g. RD/FRD, PROPIN, ITAR, etc. Include copyright information.

13. SUPPLEMENTARY NOTES. Enter information not included elsewhere such as: prepared in cooperation with; translation of; report supersedes; old edition number, etc.

14. ABSTRACT. A brief (approximately 200 words) factual summary of the most significant information.

15. SUBJECT TERMS. Key words or phrases identifying major concepts in the report.

16. SECURITY CLASSIFICATION. Enter security classification in accordance with security classification regulations, e.g. U, C, S, etc. If this form contains classified information, stamp classification level on the top and bottom of this page.

17. LIMITATION OF ABSTRACT. This block must be completed to assign a distribution limitation to the abstract. Enter UU (Unclassified Unlimited) or SAR (Same as Report). An entry in this block is necessary if the abstract is to be limited.

Final Report for Manipulating the Interfacial Electrical & Optical Properties of Dissimilar Materials with Metallic Nanostructures (FA9550-10-1-0182)

Seth R. Bank
University of Texas at Austin
sbank@ece.utexas.edu

1. Project Overview

The future of AF sensing is multi-modal imaging sensors that vertically integrate an ever increasing diversity of modes (wavelength bands, polarization states, phase, etc.) onto each pixel. Each mode is individually addressable and – ideally – dynamically reconfigurable to address the immediate situation. A number of important challenges in heterogeneous materials integration must be overcome to realize this vision. In particular, manipulating the electrical and optical properties at the interface of dissimilar materials is essential for high-performance photodetection, buses for electronic readout, polarization selectivity, and dynamic tunability.

We sought to address these challenges through the integration of precisely controlled (semi)metallic nanostructures into the heterogeneous semiconductor device structure. Metal/semiconductor interfaces are, perhaps, the most fundamental building block of solid-state devices; however, because of interfacial stability issues and difficulties in epitaxial overgrowth, they are typically relegated to metal contacts, surface gratings, and other surface structures. An exciting alternative is the rare-earth monopnictides (*e.g.* ErAs or ErSb), which may be epitaxially integrated as semimetallic nanoparticles or films into semiconductors. However, when these materials are grown as self-assembled nanostructures there is little lateral control over placement and size distribution, as well as poor electrical interconnection; conversely, the III-V overgrowth of full films is plagued by planar defect formation, which arises from the rotational symmetry mismatch, compromising optical quality (this is akin to the well-established challenges associated with GaAs growth on silicon).

Our approach to surmount these challenges began with coupling these metallic nanostructures with growth on patterned templates. We developed a patterning/regrowth process and characterized the deposition of ErAs on a variety of template surfaces using a variety of electrical, optical, structural, and chemically-sensitive techniques. Using full-wave optical simulations, we developed several alternate approaches to achieve similar optical functionality and have begun to implement them experimentally.

We also examined the optical quality of III-V layers grown above ErAs nanostructures, which is critical for future device applications, and initially found significant degradation of the III-V layers. We traced this effect back to unintentional Er incorporation into the subsequent III-V layers and developed a method to mitigate this effect using a subsurface layer of buried ErAs nanoparticles to sink the surface Er, preventing it from incorporating into the subsequent III-V layers. With this method, we achieved optical quality within 80-95% of nominally-identical Er-free structures. We also extended this work to another rare earth species, lutetium, which exhibited qualitatively similar behavior.

These integration studies inadvertently led us to the invention of a technique to grow GaAs that is free of planar defects on full films of ErAs. Specifically, we employed a seed layer of buried ErAs nanostructures, capped with a thin GaAs spacer, and used diffusion to drive incident Er subsurface. The ErAs layer growth then proceeded sub-surface, with a GaAs capping layer floating above. The advantage of this technique is that the GaAs capping layer remains registered to the underlying substrate, preventing planar defect formation during subsequent III-V growth. We thoroughly characterized the structural and electrical properties of these structures and this technique was further refined in a separate Add-On program.

We also performed initial experiments to investigate the growth of films of other rare-earth monopnictides (beyond ErAs), as well as mixed rare-earth alloys (*e.g.* LaLuAs) and find they offer broad diversity in spectral transparency and plasma frequency. These results were another highlight "spinoff" of the program and became a fundamental underpinning of a subsequent AFOSR Quantum Metamaterials and Metaphotonics (QMM) MURI program.

In addition to the research results, this program provided support for one postdoctoral scholar, and was instrumental in supporting the research activities of 3 graduated Ph.D. students, as well as 3 on-going Ph.D. students.

2. Growth on Nanotemplated Surfaces

2.1 Nanotemplating and Epitaxial Regrowth Progress

We began by developing templating and regrowth processes, which required significant hardware modifications to the molecular beam epitaxy (MBE) system. A representative set of scanning electron micrographs are shown in **Figure 1**, illustrating the successful templating of GaAs trenches for ErAs nanowire regrowth. The key hardware modification is the atomic hydrogen cleaning source, shown in **Figure 2**, which we installed on the buffer chamber of the MBE system for cleaning the templates immediately prior to introduction into the MBE growth chamber.

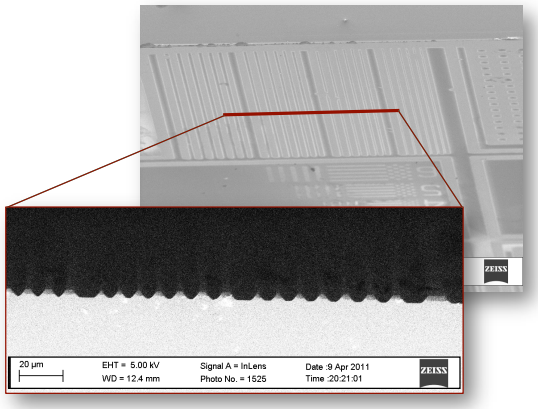

Figure 1. Overhead and cross-sectional scanning electron micrographs (SEM) of the nanotemplates. Facets from the etching process are well-defined and surface contaminants, such as photoresist residue, are not observed.

Figure 2. Photograph of the atomic hydrogen cleaning station installed on the MBE system for substrate cleaning, prior to epitaxial regrowth. The hydrogen feed gas is purified using a palladium purifier (not shown). A residual gas analyzer enables real-time characterization of the wafer surface during cleaning, by monitoring the desorbing species.

To avoid contaminating the molecular beam epitaxy (MBE) chamber during growth, great care must be taken during the processing of the GaAs substrates prior to loading into the ultra-high vacuum (UHV) chamber. The process flow, using photolithography and etching to reveal a growth surface with a series of V-grooves, is described in **Figure 3**. First, Si_3N_4 films are deposited on the front and back surfaces of the GaAs substrates to act as a hard mask by covering the GaAs surfaces during photolithography, protecting the GaAs surface from contamination with photoresist. Photoresist is then spun on to the Si_3N_4, exposed to reveal the pattern of lines on the lithography mask, and then developed. The lithography patterns are transferred onto the Si_3N_4 mask by etching in hydrofluoric acid, and then the

photoresist is removed using acetone. A 10 second GaAs etch of H_2S0_4:H_2O_2:H_20 is then used to create the V-grooves in the GaAs substrate. After the V-grooves have been etched, the remaining Si_3N_4 is etched away, eliminating any residual photoresist from the patterned substrate, prior to regrowth.

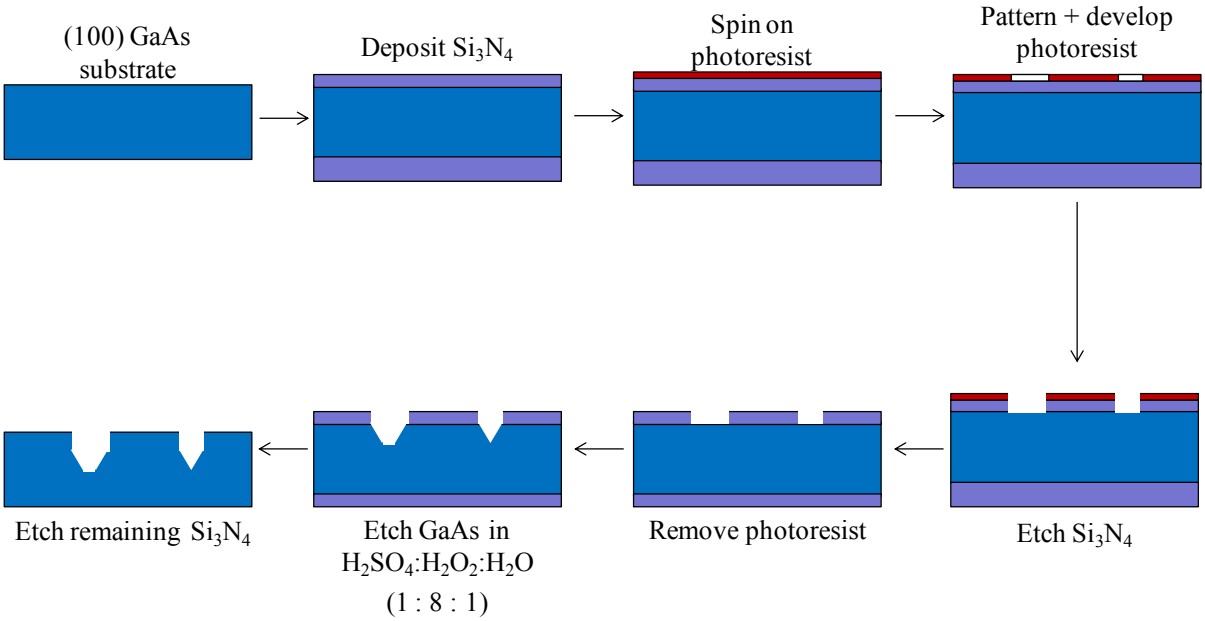

Figure 3. Process flow for forming V-grooves in GaAs substrates. Si_3N_4 encapsulation and hard masking, which are removed prior to regrowth, are essential for completely removing photoresist prior to MBE regrowth.

We examined a number of etch chemistries, but focus on H_2S0_4:H_2O_2:H_20 for succinctness. We fabricated grooves of different widths and pitches, with representative images shown in **Figure 4a** and **4b**. When the samples were examined in a scanning electron microscope (SEM), the images revealed triangular features on the sidewalls near the tops of the mesas as shown in **Figure 4c**. A photograph of a regrowth sample after atomic hydrogen treatment, but prior to regrowth, is shown in **Figure 4d**.

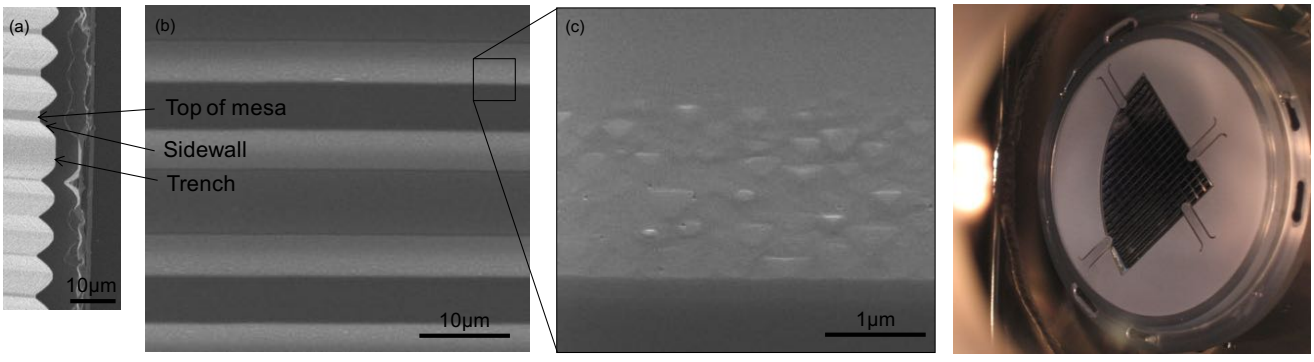

(a) (b) (c) (d)

Figure 4. (a) Cross-sectional SEM image of the patterned sample, (b) plan-view SEM image of the sample after nanoparticle growth, showing the tops of the mesas, the sidewalls, and the trenches in between, (c) high magnification SEM image showing triangular features on the sidewalls near the tops of the mesas, and (d) photograph of patterned substrate, in the MBE buffer chamber, during atomic hydrogen cleaning.

To determine if the triangular features were a result of defects introduced during processing, we examined the samples after etching, prior to regrowth. SEM images of the samples etched using the H_2S0_4:H_2O_2:H_20 (1:8:1) solution are shown in **Figure 5**. The regions of increased roughness are visible on the (111) sidewalls. These regions of increased roughness could have contributed to the triangular features that were observed following regrowth (**Figure 4c**).

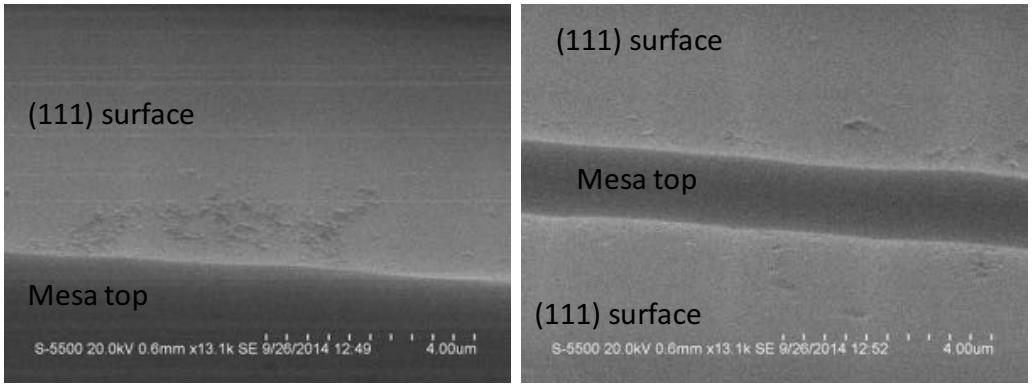

Figure 5. SEM images of GaAs wafers after etching in a H_2S0_4:H_2O_2:H_20 (1:8:1) solution. Regions of increased roughness are visible on the (111) surfaces that make up the mesa sidewalls.

Since the H_2S0_4:H_2O_2:H_20 (1:8:1) solution did not result in smooth (111) sidewalls, we tested different ratios of the H_2S0_4:H_2O_2:H_20 solutions, including 3:8:3, and 3:8:1. For the H_2S0_4:H_2O_2:H_20 (3:8:3) solution, the SEM images showed noticeable defects on the (111) sidewalls, as shown in **Figure 6**. Since this etch did not produce smooth, defect-free sidewalls after etching, we did not attempt regrowth on this sample.

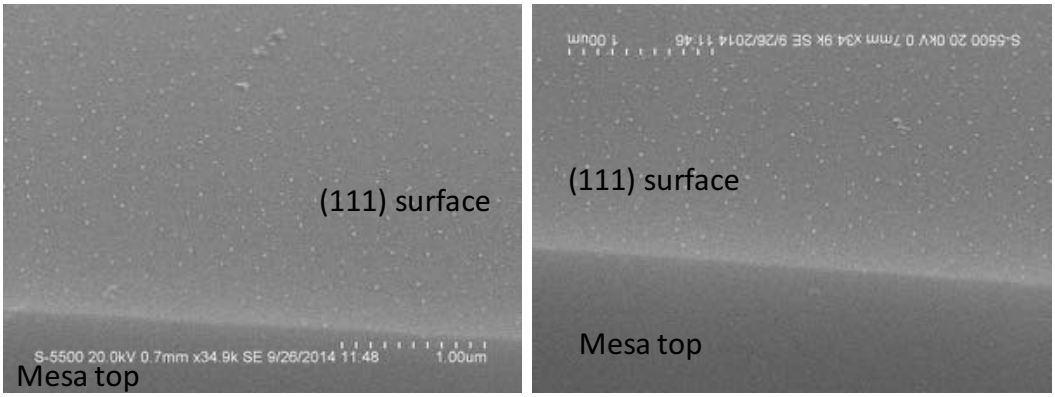

Figure 6. SEM images of GaAs wafer etched in a solution of H_2S0_4:H_2O_2:H_20 (3:8:3), showing the top of the mesa and the (111) surface of the sidewalls. The roughened (111) surfaces are unsuitable for regrowth.

Etching the GaAs wafers in the H_2S0_4:H_2O_2:H_20 (3:8:1) solution resulted in samples with undercut mesas. SEM studies revealed that the majority of the mesas were undercut, and a few of the thicker mesas are only faintly visible. Since the H_2S0_4:H_2O_2:H_20 (3:8:1) solution etched away the majority of the mesas, making this etch chemistry also unsuitable for regrowth.

2.2 Characterization of MBE Regrowth Process

One of the key considerations with epitaxial regrowth is to avoid contaminating the MBE system. Using our "standard" InGaAs/GaAs quantum well (QW) as a sensitive probe of the optical quality, we compared the luminescence efficiency of QW structures grown immediately prior to and immediately after an epitaxial regrowth experiment. The photoluminescence (PL) results are summarized in **Figure 7**, where we find that the optical quality actually improves after regrowth, indicating that epitaxial regrowth does not contaminate the MBE system. This is critical for future device integration and also to prevent inadvertent damage to the MBE system.

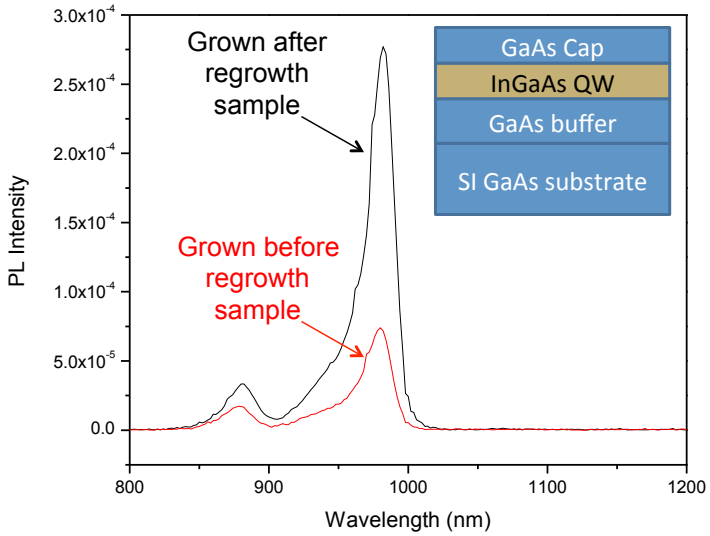

Figure 7. Photoluminescence results from nominally-identical InGaAs/GaAs test structures grown immediately before (**red**) and immediately after (**black**) an epitaxial regrowth run. Note the surprising improvement, which shows that the MBE system is not adversely affected by epitaxial regrowth experiments. Inset: Layer structure of InGaAs/GaAs QW test structure.

2.3 Characterization of ErAs Deposited on Templated Surfaces

After honing the etch chemistry to mitigate the roughening of the (111) facets and determining that regrowth did not contaminate the MBE system, we began to characterize regrown samples. To achieve high resolution imaging, we employed tapping-mode atomic force microscopy (AFM) to compare the surface topography of the planar regions and the sidewalls, since previous AFM images of uncapped ErAs nanoparticles on (001) GaAs revealed a roughening in the GaAs surface due to the embedding of the ErAs nanoparticles (**Figure 8a**). AFM images of the patterned substrates after ErAs nanoparticle deposition revealed an increased number of features on the (111) sidewalls in comparison to the (001) surface, as shown in **Figures 8b** and **8c**. These features were initially believed to be the ErAs nanoparticles.

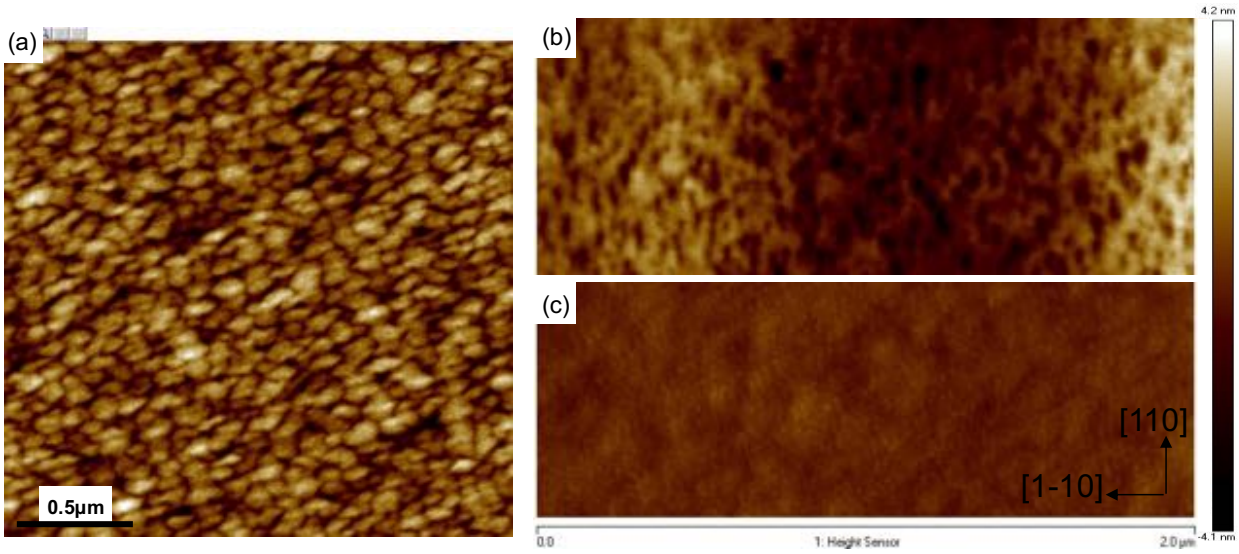

Figure 8. (a) Tapping mode AFM images of uncapped 1 monolayer (ML) ErAs nanoparticles on (a) unetched (001) GaAs, (b) etched (111) GaAs, and (c) etched (001) GaAs.

Prior conductive-AFM (CAFM) studies of ErAs capped with 1.5 nm of GaAs revealed regions of dramatically increased current density corresponding to the ErAs nanoparticles [1]. To determine if the features observed in the tapping mode AFM images from the V-groove sidewalls were the nanoparticles, or artifacts due to etching and regrowth, we grew nanoparticle samples for CAFM studies. The samples were grown on n-doped (001) GaAs substrates that were processed and patterned using the procedure described above. Following the growth of a 200 nm GaAs buffer, 1 ML ErAs nanoparticles were deposited at 530^{o}C, and capped with 1.5 nm of p-doped GaAs, similar to previous experiments on planar (001) GaAs. A representative CAFM image from these samples is shown in **Figure 9**. It revealed regions of increased current density on the (111) sidewalls, but the depth of the V-grooves was ~ 1 µm, making CAFM scanning of the grooves extremely challenging.

Figure 9. CAFM image of (111) sidewalls after deposition of 1 ML ErAs nanoparticles capped with 1.5 nm GaAs.

We continued to pursue AFM and conductive AFM studies, with our best results summarized in **Figure 10.** The key challenge is the large topographical height variation, due to the V-groove geometry, which makes AFM-based approaches nearly impossible in practice. Particularly challenging is getting the tip of the AFM physically into the bottom of the groove. We further examined other GaAs etch chemistries to realize smoother GaAs overgrowth and to minimize the presence of triangular features and

pits on the (111) sidewalls, but the amplitude variation remained too great. After many different approaches to surmount this issue, including machining a variety of angled chucks to make the sidewalls "flat," we concluded that AFM and CAFM are not effective characterization techniques for this purpose.

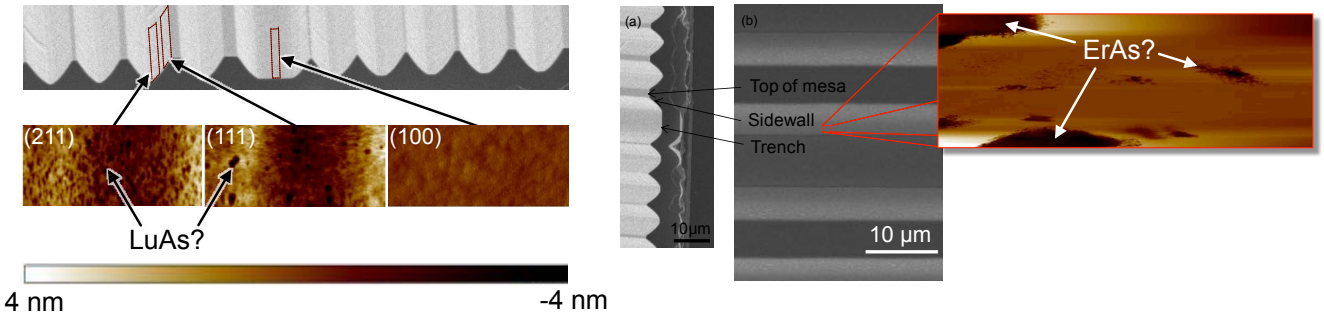

Figure 10. Summary of scanned probe studies of growth on V-groove templates. (a) Topographical AFM and (b) conductive AFM scans from various sidewalls and trenches. Scan locations are indicated on (grey) SEM images.

Given the difficulty in discerning the nanoparticle location using AFM and CAFM, we began to use energy-dispersive X-ray spectroscopy (EDS) to perform chemically-sensitive analysis, as well as optical characterization. **Figure 11** plots SEM and EDS images of a single V-groove collected with a Hitachi S5500 SEM, imaging at 25 kV (spatial resolution nominally ~5 nm). EDS images were collected in with a Bruker Quantax 200 using a XFlash 5 EDS detector. As seen in the images, particularly **Figure 11d**, there did not appear to be any spatial ordering of the ErAs nanostructures, given what appears to be a randomly distributed erbium signature.

To study the optical properties of ErAs deposited on templated substrates, spatially-resolved reflectivity spectra were collected with the 36x objective of a Bruker Hyperion 1000 IR microscope and spectrally-resolved with a Bruker Vertex 80V vacuum FTIR. Line scan reflectivity spectra, normalized to the reflectivity of a gold standard, are plotted in **Figure 12**. These are 75 line scans taken 1.023 µm apart. We attribute the abrupt rise in reflectivity beyond ~15 µm to the plasma frequency of the n-type GaAs substrate. At shorter wavelengths, there are a variety of pronounced spectral features that are significantly more pronounced in the samples with ErAs (**Figure 12b** and **12c**) than the control without ErAs (**Figure 12a**). While this is very encouraging, though we do not yet know if these are truly due to wire formation or simply increasing the surface reflectivity, due to the large magnitude of the ErAs dielectric constant at these wavelengths. Polarization-resolved measurements are required to provide relatively direct evidence; it is expected that reflectivity would be dramatically different for light polarized perpendicular and parallel to the V-grooves.[1]

[1] Unfortunately, we encountered difficulty mechanically actuating the polarizer on the IR microscope and have been working with the vendor on a solution; unfortunately, this issue has not yet been resolved.

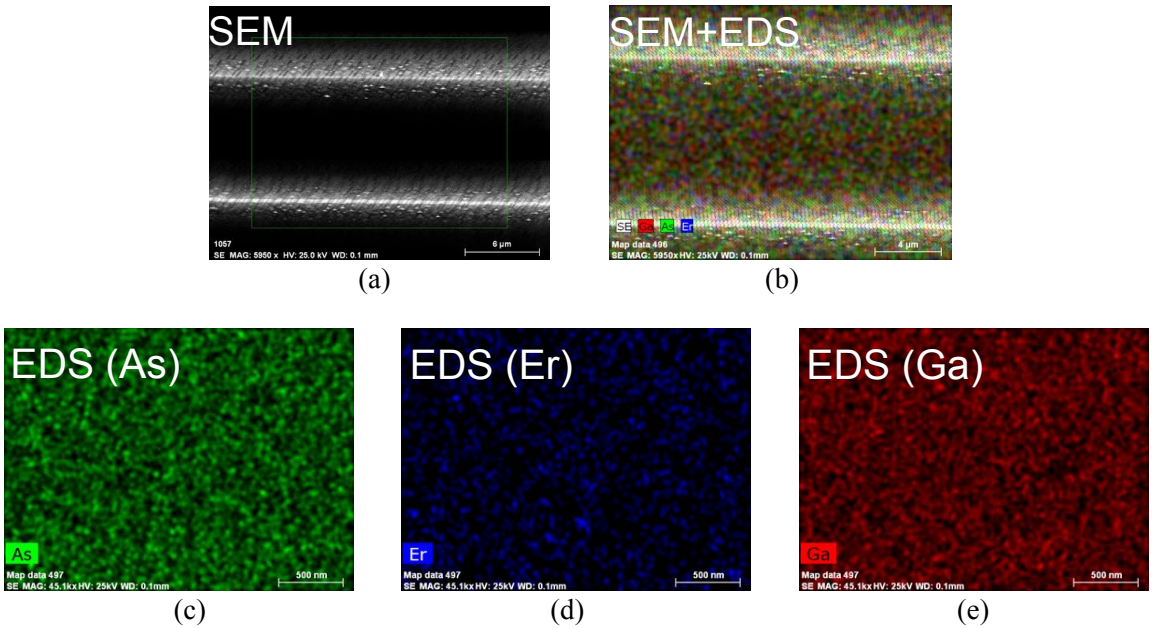

Figure 11. (a) Top-view SEM image of V-groove following 1 ML of ErAs deposition, (b) Overlay of SEM and EDS images, (c) arsenic EDS map, (d) erbium EDS map, and (e) gallium EDS map. Erbium profile appears random, at least to within the ~5 nm spatial resolution of the EDS system. TEM could offer higher spatial resolution.

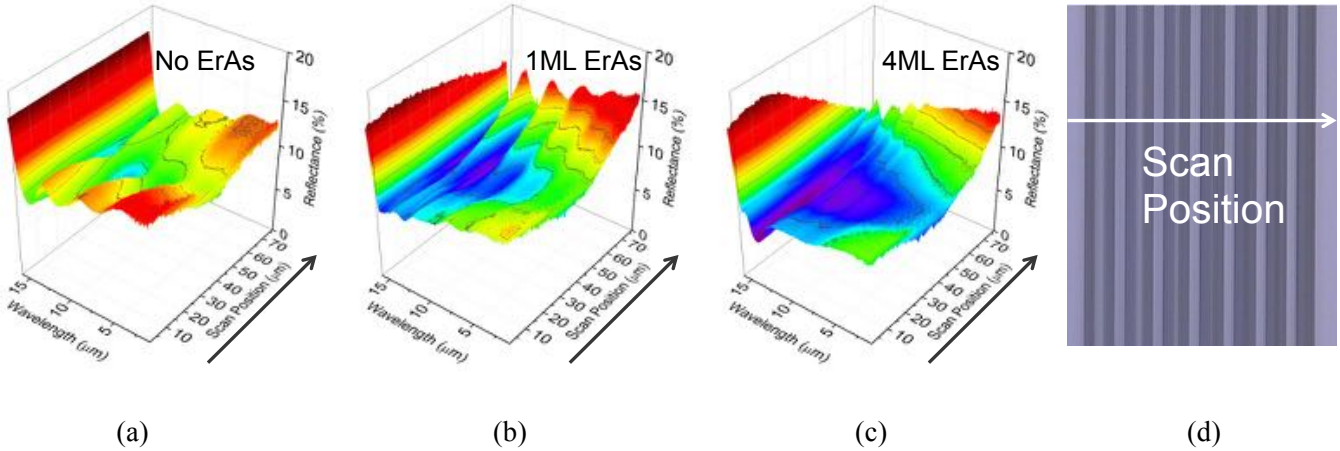

Figure 12. Optical reflectivity of V-groove structures, as a function of wavelength and position, measured with a FTIR and IR-microscope. (a) Patterned ErAs-free control, (b) 1 ML equivalent ErAs deposition, (c) 4 ML equivalent ErAs deposition, and (d) plan-view microscope image showing the measurement direction. Arrows indicate the scan direction.

2.4 Alternative Materials for Growth on V-Groove Templates

Given the challenges we encountered on the metrology front, we began to consider alternative material systems that could provide similar functionality as ErAs. We have identified an attractive approach, based on the lateral epitaxial overgrowth (LEO) technique [2] illustrated in **Figure 13a**. The LEO technique is commercially very important for III-N LED growth; despite being first demonstrated in GaAs [2], however, it has not found application in conventional III-V materials. Our full wave calculations indicate that such structures can produce plasmonic-like response (**Figure 13b**), as well as spectrally-

selective perfect transmission (**Figures 13c** and **13d**) and near perfect reflection (**Figure 13d**), depending upon the grating dimensions.

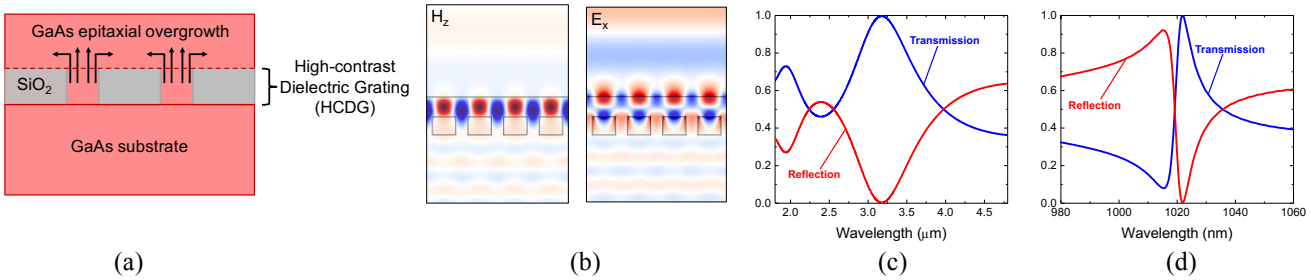

Figure 13. (a) Cross-section of optical test structure where the width and pitch of an epitaxially-integrated SiOx/GaAs grating can be varied to produce strong spectral response features. (b) Illustrative mode patterns for the magnetic and electric fields calculated with MEEP. By tuning the grating pitch and width, the optical response can be tuned into the (c) mid-IR and (d) near-IR, depending on the application.

We extended this work to identify ways to integrate plasmonic response into high-contrast regrown structures. As part of an orthogonal (but complementary) AFOSR MURI, we have extensively studied the growth of highly-doped InAs, which acts as a metal in the mid- and far-infrared (depending on the doping level) and investigated the response of doped InAs wires inserted into the V-grooves. Growth of In(Ga)As in V-grooves has been extensively studied as a method for fabricating nanowire lasers and served as the initial motivation for our proposed work. Combining MBE growth of InGaAs nanowires on V-grooves [3] and modulation doping of nanowires in V-grooves [4] could yield highly conductive, low effective mass, wires that would function as metals in the mid-infrared. **Figure 14** illustrates this idea. The top plot is a cross-sectional carrier density map of an In(Ga)As nanowire grown on a modulation-doped V-groove, calculated through 2-D Poisson's equation, based on the electrostatic permittivity and heterostructure potential distribution of the material system. Numerical solutions were approximated using the 2-D finite difference method to compute the Laplace operator and tested for convergence. The plots below are 1-D band diagrams and charge density plots, showing that the In(Ga)As wire should act metallic at shorter wavelengths than the remainder of the structure, affording a spectral window for exploiting new optical functionality from buried arrays of metallic nanostructures.

3. Film and Nanostructure Integration with III-V's

3.1 Optical Quality Studies Integrating ErAs with III-V's

Using an InGaAs quantum well as a sensitive probe of the optical quality of the III-V overgrowth over a layer of ErAs nanostructures (**Figure 15a**), we have demonstrated for the first time that high-quality III-V materials can be integrated within 15 nm from a layer of ErAs nanostructures, without degradation of their optical quality (**Figure 15b**). The key issue that we surmounted was the unintentional incorporation of erbium into the overgrown epitaxial layers, which act as fast non-radiative centers.

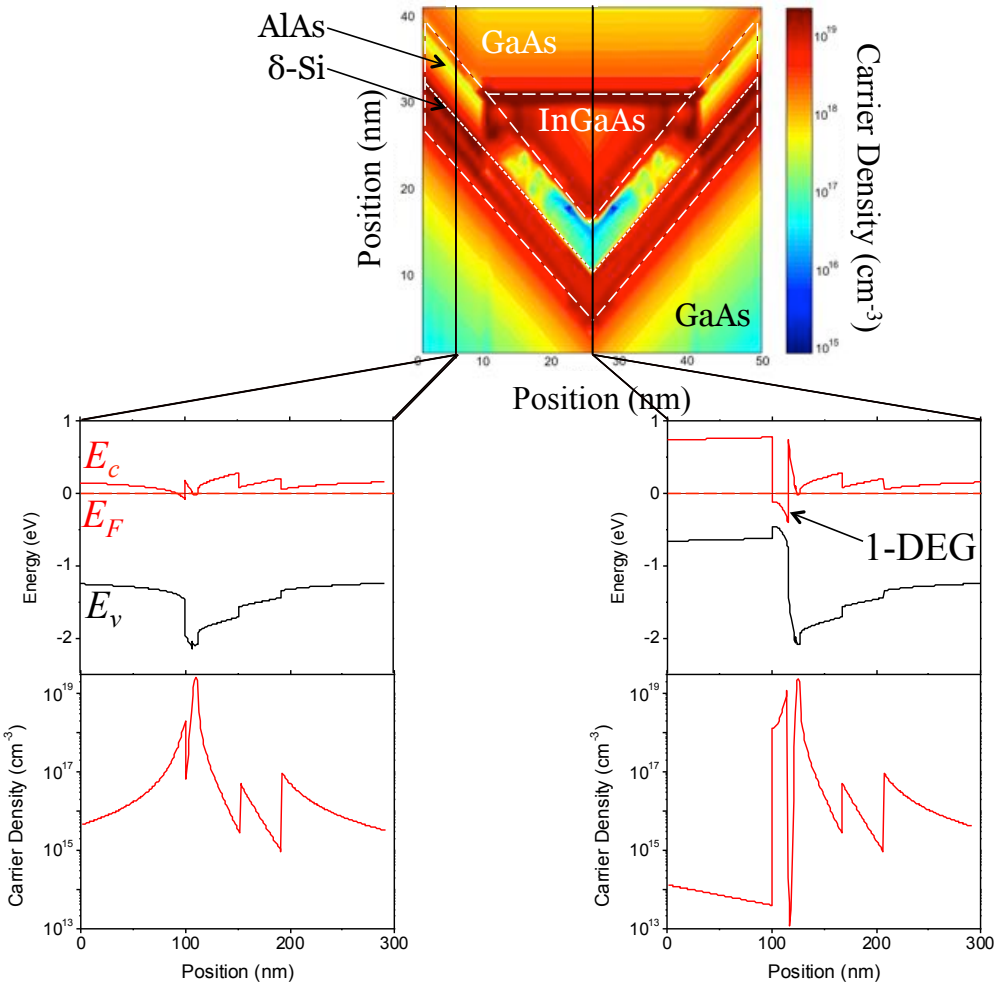

Figure 14. (Top plot) Cross-sectional view of a modulation-doped InGaAs V-groove nanowire. Color corresponds to calculated carrier concentration, determined from 2-D Poisson simulations. (Bottom plots) 1-D cuts through the structure plotting band diagrams and local charge density. As seen on the right, excellent 1-D electron gas (1-DEG) structures should be achievable and would be expected to function as metal nanowires in the mid-infrared.

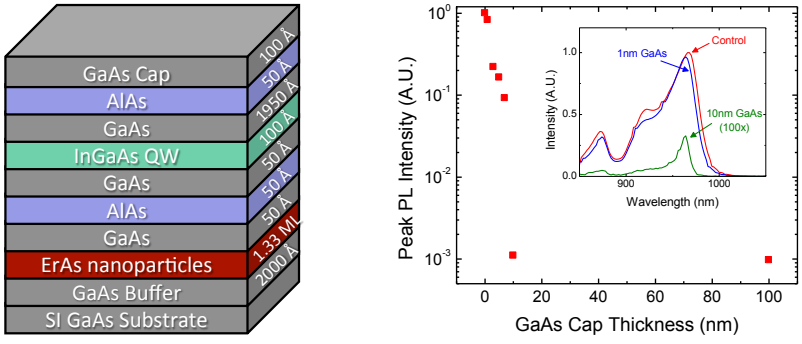

(a) (b)

Figure 15. (a) Layer structure and (b) photoluminescence (PL) results for the optical overgrowth studies. With proper management of the erbium source, the PL strength of the InGaAs QW grown 15 nm above a layer of ErAs nanostructures was 95% of that from the ErAs-free control. Inset: Key PL spectra.

3.2 Novel ErAs Embedded Film Growth Method

Using the insights that we gained in the optical quality studies, we invented an entirely new growth mode for epitaxial (semi)metallic films, integrated with high-quality III-V semiconductors. This breakthrough is particularly critical to the future of multi-modal sensors, specifically vertically integrating a diversity of sensing modes onto a single "pixel." In such devices, it is highly desirable that electrical contact can be made independently to each detector in the pixel stack for electrical readout – requiring transparent, epitaxially-compatible, electrical conductors. While ErAs and many of the other rare-earth monopnictides (generally denoted as RE-V) can be grown epitaxially on zinc-blende III-V substrates, the rotational symmetry mismatch between the III-V and ErAs results in a high density of planar defects when III-V is grown on a film of ErAs, akin to the challenges associated with GaAs growth on silicon.

We circumvented this "fundamental" obstacle using a seed layer of buried ErAs nanostructures. In the method, sketched in **Figure 16**, the ErAs layer growth proceeds sub-surface, with a GaAs capping layer floating on top. This capping layer remains registered to the underlying substrate, preventing planar defect formation during subsequent III-V growth. The benefits are clearly observed in the transmission electron microscopy images shown in **Figure 17**, where planar defect formation is strongly inhibited with even a 1 nm GaAs capping layer.

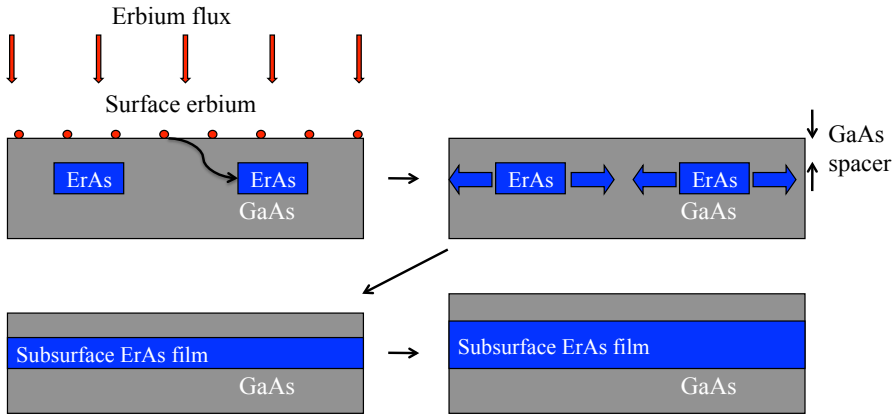

Figure 16. Schematic of the film growth process employing a layer of buried ErAs nanostructures as a seed for film growth. The surface GaAs layer 'floats' on the ErAs film and remains registered to the underlying GaAs substrate, preventing planar defect formation during subsequent III-V growth.

Temperature-dependent resistivity measurements confirmed our hypothesis that this growth mode indeed produces continuous films. **Figure 18a** plots the temperature dependence of 5 and 10 monolayer (ML) thick films of ErAs, grown by the embedding mechanism [5]. Resistivity increased gradually with temperature, consistent with a continuous metal layer and quite distinct from the behavior of interconnected islands. As shown in **Fig. 18b**, the resistivity of interconnected islands is known to decrease rapidly with temperature, due to thermally-activated hopping transport [6]. Therefore, we can safely conclude that we have indeed grown continuous films of ErAs with the seeded growth technique.

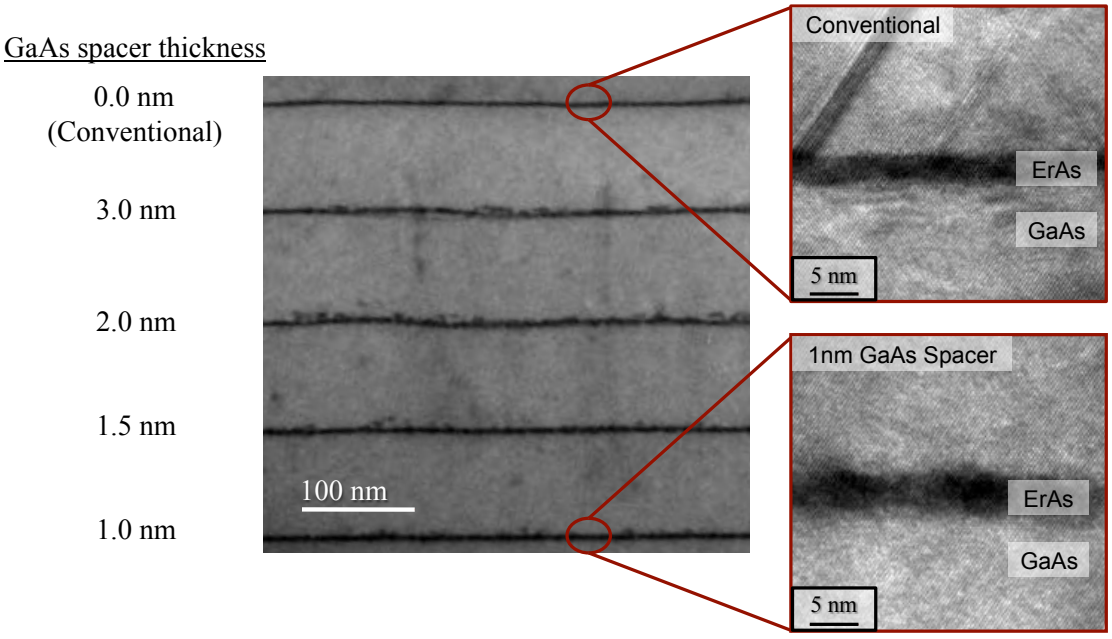

Figure 17. Transmission electron microscopy (TEM) image of five monolayer thick ErAs films, grown using various GaAs spacer thicknesses. Insets: High-resolution TEM images. Note that planar defect formation has been inhibited using a 1 nm GaAs spacer, as compared with the layer grown by the conventional growth technique (0 nm spacer).

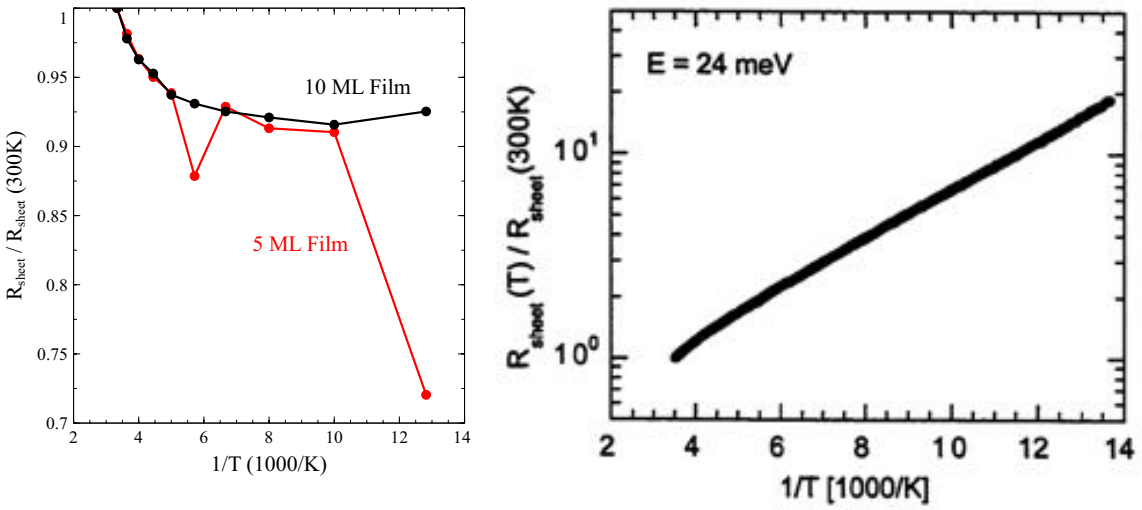

Figure 18. Temperature dependent resistivity of (a) ErAs films of 5 and 10 monolayer (ML) thickness, grown by the embedded growth mode and (b) 1.8 ML of ErAs shown for comparison [6]. The ErAs films grown by the embedding mechanism behavior are consistent with that of a continuous semimetallic layer clearly inconsistent with the behavior of interconnected islands shown in (b).

3.3 Towards Other Materials for Embedded Metal Contacts

Building on our success using the embedded film technique [7] to integrate ErAs films into high-quality GaAs, we began to examine other rare earth monopnictide compounds and alloys to understand the diversity of material properties they afford (e.g. different spectral transmission windows). To this end, we investigated alloys of LaLuAs films and found they offer broad diversity in spectral transparency and

plasma frequency. **Figure 19** plots the transmission spectra for LaAs, LuAs, and also $La_{0.48}Lu_{0.52}As$, which is lattice-matched to InP. Note the significant diversity in spectral transmission windows. As seen in the EDS scan shown in **Figure 20**, as well as the X-ray diffraction in **Figure 21**, these alloys appear to be quite uniform and of high-quality. These results are a highlight "spinoff" of the program and became a fundamental underpinning of our portion of the subsequent AFOSR MURI Quantum Metamaterials and Metaphotonics (QMM) program.

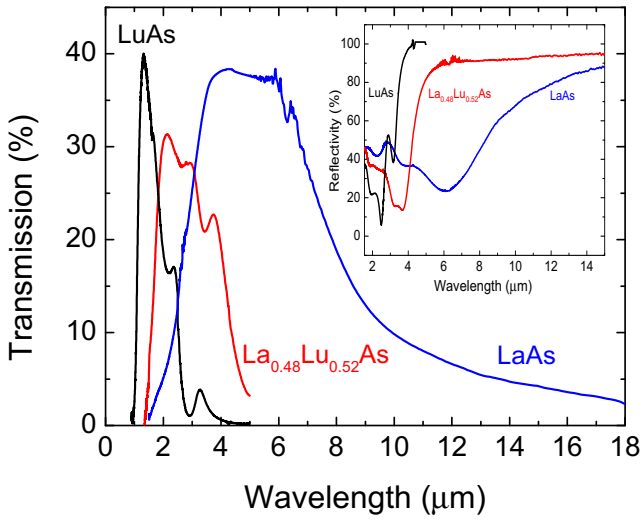

Figure 19. Transmission (Inset: reflectivity) spectra for LuAs, $La_{0.48}Lu_{0.52}As$, and LaAs films. Note the dramatic diversity in optical properties afforded by varying the composition.

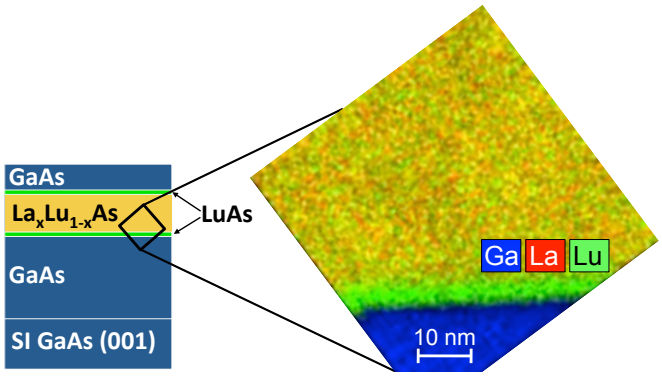

Figure 20. Chemical composition map of $La_{0.48}Lu_{0.52}As$ film taken with energy-dispersive X-ray spectroscopy (EDS) in a TEM for chemically-sensitive analysis. Note that the film is homogenous, at least to within the 1-2 nm spatial resolution of the instrument.

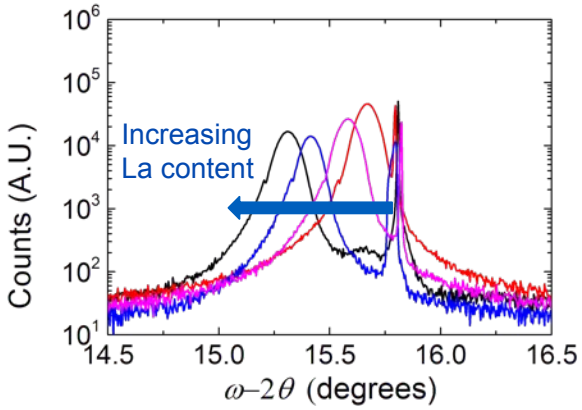

Figure 21. ω-2θ X-ray diffraction scans of LaLuAs films of varying composition. Note the shift in the LaLuAs peak with increasing composition, indicating that the lattice constant increases.

3.4 Optical Integration Studies of Other Rare Earth Materials

As a precursor to applying the embedded-film growth method to other rare earth monopnictides, we performed studied the unintentional incorporation of lutetium (Lu), using methods similar to those described in **Section 3.1**, since LuAs grows quite similarly to ErAs. We found qualitatively similar behavior for Lu as Er and were able to sink lutetium with subsurface LuAs nanoparticles to maximize the optical quality of III-V layers grown above; however, we found that the diffusivity is significantly lower for Lu than Er. This has important ramifications for future device integration and is somewhat surprising, given that Lu is a smaller atom than Er. Future work should, therefore, focus on lower atomic number rare earth elements, which may exhibit larger diffusion coefficients, enabling the growth of thicker embedded films and higher quality III-V layers grown subsequently.

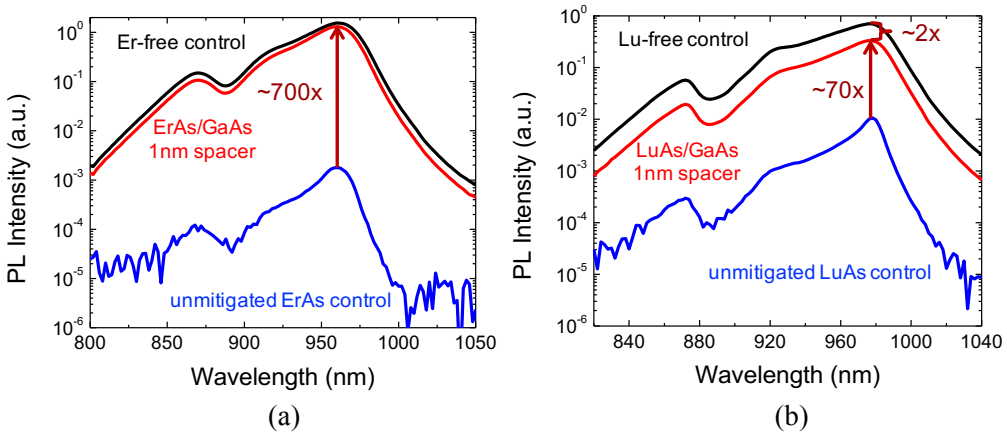

Figure 22. (a) Sinking surface Er with buried ErAs nanostructures recovered the peak PL to within 20% of the Er-free control. (b) Sinking surface Lu with buried LuAs nanostructures increased PL by ~70x, but remained ~2x lower than the Lu-free control.

Photoluminescence spectroscopy was performed on samples similar to those of **Figure 15a** under room-temperature conditions at an excitation-density of ~2.4 kW/cm^2 and their PL spectra are compared in **Figure 22**. In particular, we observed substantial PL improvement of ~70x by sinking the Lu with an underlying layer of LuAs nanoparticles. Also, compared to the Lu-free control, Lu-sinking was able to

recover PL to within a factor of 2x of an entirely Lu-free control. However, comparing LuAs/GaAs system to ErAs/GaAs, there is a quantitative departure from the case of Er in that the peak PL efficiency could be recovered to within 20% of the Er-free control.

Further probing these differences, we grew additional structures varying the GaAs spacer thickness, choosing 5nm and 100nm spacer to determine the impact of Lu diffusion as a function of spacer thickness as the cause for peak PL reduction in the LuAs/GaAs system. Comparing the cases of Lu and Er, as functions of the GaAs spacer thickness, we found another departure of the LuAs/GaAs system from ErAs/GaAs as seen in **Figure 23a**. As the GaAs spacer thickness was varied from 1 nm to 10 nm in the ErAs/GaAs system, several orders of magnitude reduction in peak PL intensity was observed. Applying Fick's law of diffusion model under limited source conditions [8], the estimated diffusion depth of Er through GaAs is approximately 2.1 nm. However, when varying GaAs spacer thickness for Lu, a more rapid decline in peak PL intensity was observed, reaching close to the diffusion limit when employing a ~5nm GaAs spacer. Fitting the peak PL response to a limited source diffusion model, the estimated Lu diffusion length through GaAs is approximately 1.3 nm, ~50% less than Er in GaAs.

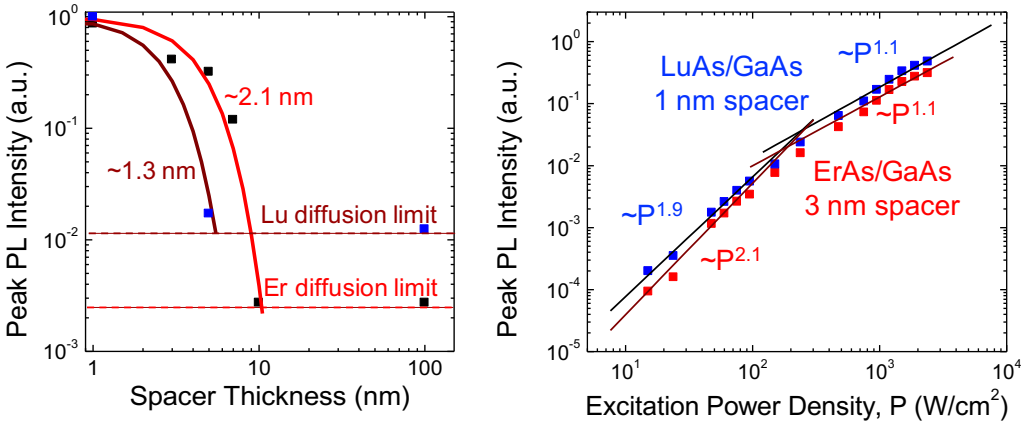

Figure 23. (a) Diffusion models fit to GaAs spacer variation suggested limited Lu diffusion through GaAs than Er. (b) LuAs/GaAs system with 1nm spacer close matches the ErAs/GaAs system with 3nm spacer also suggests residual Lu incorporation in its emitter region.

Based on the diffusion analysis, a close analog to the LuAs/GaAs system employing a 1 nm GaAs spacer was found in ErAs/GaAs system employing a 3 nm spacer. Since it is just outside its diffusion length of 2.1 nm, this sample has a large degree of Er incorporation in the emitter. In performing excitation-density-dependent PL, as seen in **Figure 23b**, we see that the PL response of LuAs/GaAs 1 nm spacer system closely matches using ErAs/GaAs 3 nm spacer systems, further confirming that peak PL reduction in the LuAs/GaAs 1 nm spacer system is due to Lu incorporation as a result of more limited Lu diffusion through GaAs.

4. Patents

None – it is unfortunately difficult to enforce a "process" driven patent, so patenting the "nanoparticle-seeded" ErAs embedded film growth technique did not seem appropriate.

5. Awards

- (Supervisor) MRS Electronic Materials Conference (EMC) Student Paper Award (2014)

  - Awarded to the 1-3 best student papers
- (Supervisor) IEEE Device Research Conference (DRC) Student Paper Award (2013)
  - Awarded to the 2 best student papers
- (Supervisor) Ben Streetman Research Prize (2013)
  - Best contribution by UT Ph.D. student to electronic/photonic materials/devices
- (Supervisor) MRS Electronic Materials Conference (EMC) Student Paper Award (2012)
  - Awarded to the 1-3 best student papers
- (Supervisor) Ben Streetman Research Prize (2012)
  - Best contribution by UT Ph.D. student to electronic/photonic materials/devices
- IEEE Senior Member (2012)

6. Personnel Supported

A number of Ph.D. researchers were involved at various points in the research; the key personnel involved in this program were:

- Dr. Vaishno Dasika (Postdoc) – Moved to Texas Instruments
  - All epitaxial regrowth development and scanned-probe microscopy studies
- Dr. Erica Krivoy (Ph.D. graduate) – Moved to DDM systems (additive manufacturing start-up)
  - Film growth and optical characterization
- Dr. Adam Crook (Ph.D. graduate) – Lockheed Martin (photodetector R&D)
  - Initial optical integration and buried film growth
- Dr. Rodolfo Salas (Ph.D. graduate) – MIT Lincoln Labs (full-time research staff)
  - SIMS studies of metal-semiconductor integration (not discussed in report)
- Nathanial Sheehan (current Ph.D. student)
  - Follow-on epitaxial regrowth and EDS studies
- Kyle McNicholas (current Ph.D. student)
  - Film growth and optical characterization
- Daniel Ironside (current Ph.D. student)
  - Optical simulations and PL studies

7. Journal Publications[2]

1. K.W. Park, E.M. Krivoy, H.P. Nair, S.R. Bank, and E.T. Yu, "Cross-sectional scanning thermal microscopy of ErAs/GaAs superlattices grown by molecular beam epitaxy, " *Nanotech.*, vol. 26, pp. 265701-1-5, June 2015.

2. X. Li, V. D. Dasika, P.-C. Li, S.R. Bank, E.T. Yu, "Minimized open-circuit voltage reduction in GaAs/InGaAs quantum well solar cells with bandgap-engineered graded quantum well depths, " *Appl. Phys. Lett.*, vol. 105, no. 12, pp. 123906, Sept. 2014.

3. E.M. Krivoy, S. Rahimi, H.P. Nair, R. Salas, S.J. Maddox, D.J. Ironside, Y. Jiang, G. Kelp, G. Shvets, D. Akinwande, and S.R. Bank, "Growth and characterization of single crystal rocksalt LaAs using LuAs barrier layers," *Appl. Phys. Lett.*, vol. 101, no. 22, pp. 221908, Nov. 2012.

[2] Not listed: three manuscripts in progress.

4. K.W. Park, V.D. Dasika, H.P. Nair, A.M. Crook, S.R. Bank, and E.T. Yu, "Conductivity and structure of ErAs nanoparticles embedded in GaAs pn junctions analyzed via conductive atomic force microscopy," *Appl. Phys. Lett.*, vol. 100, no. 23, pp. 233117, June 2012.

5. E.M. Krivoy, H.P. Nair, A.M. Crook, S. Rahimi, S.J. Maddox, R. Salas, D.A. Ferrer, V.D. Dasika, D. Akinwande, and S.R. Bank, "Growth and characterization of LuAs films and nanostructures," *Appl. Phys. Lett.*, vol. 101, no. 14, pp. 141910, Oct. 2012.

6. K.W. Park, H.P. Nair, A.M. Crook, S.R. Bank, and E.T. Yu, "Scanning capacitance microscopy of ErAs nanoparticles embedded in GaAs pn junctions," *Appl. Phys. Lett.*, vol. 99, pp. 133114, Sept. 2011.

7. A.M. Crook, H.P. Nair, D.A. Ferrer, and S.R. Bank, "Suppression of planar defects in the molecular beam epitaxy of GaAs/ErAs/GaAs heterostructures," *Appl. Phys. Lett.*, vol. 99, pp. 072120, Aug. 2011.

8. A.M. Crook, H.P. Nair, and S.R. Bank, "Surface segregation effects of erbium in GaAs growth and their implications for optical devices containing ErAs nanostructures," *Appl. Phys. Lett.*, vol. 98, no. 12, pp. 121108, Apr. 2011.

8. References

[1] K.W. Park, H.P. Nair, A.M. Crook, S.R. Bank, and E.T. Yu, "Quantitative scanning thermal microscopy of ErAs/GaAs superlattice structures grown by molecular beam epitaxy," *Appl. Phys. Lett.*, vol. 102, no. 6, pp. 061912, Feb. 2013.

[2] R. W. McClelland, C. O. Bozler, and J. C. C. Fan, "A technique for producing epitaxial films on reuseable substrates," *Applied Physics Letters,* vol. 37, pp. 560-62, 1980.

[3] For example, X.Q. Shen, M. Tanaka, and T. Nishinaga, "Resharpening effect of AlAs and fabrication of quantum-wires on V-grooved substrates by molecular beam epitaxy," *J. Cryst. Growth.*, vol. 127**,** no. 1-4, pp. 932-936, Feb. 1993.

[4] D. Kaufman, Y. Berk, B. Dwir, A. Rudra, A. Palevski, and E. Kapon, "Conductance quantization in V-groove quantum wires," *Phys. Rev. B*, vol. 59, R10433, April 1999.

[5] A. M. Crook, H. P. Nair, D. A. Ferrer, and S. R. Bank, "Growth of rare-earth monopnictide films via epitaxial embedding for plasmonics," *International Symposium on Compound Semiconductors (ISCS)*, June 2011, Berlin, Germany.

[6] K. Kadow, "Self-assembled ErAs islands in GaAs for photomixer devices," Ph.D. Thesis, Univ. of Calif., Santa Barbara, CA, 2000.

[7] A.M. Crook, H.P. Nair, D.A. Ferrer, and S.R. Bank, "Suppression of planar defects in the molecular beam epitaxy of GaAs/ErAs/GaAs heterostructures," *Appl. Phys. Lett.*, vol. 99, pp. 072120, Aug. 2011.

[8] W. F. Smith, *Foundations of Materials Science and Engineering*, 3rd ed., McGraw-Hill (2004).

AFOSR Deliverables Submission Survey

Response ID:6617 Data

1.

1. Report Type

Final Report

Primary Contact E-mail

Contact email if there is a problem with the report.

sbank@ece.utexas.edu

Primary Contact Phone Number

Contact phone number if there is a problem with the report

6504500060

Organization / Institution name

Univ. of Texas

Grant/Contract Title

The full title of the funded effort.

Manipulating the Interfacial Electrical & Optical Properties of Dissimilar Materials with Metallic Nanostructures

Grant/Contract Number

AFOSR assigned control number. It must begin with "FA9550" or "F49620" or "FA2386".

FA9550-10-1-0182

Principal Investigator Name

The full name of the principal investigator on the grant or contract.

Seth R. Bank

Program Manager

The AFOSR Program Manager currently assigned to the award

Dr. Ken Goretta

Reporting Period Start Date

05/01/2010

Reporting Period End Date

04/30/2016

Abstract

The future of AF sensing is multi-modal imaging sensors that vertically integrate an ever increasing diversity of modes (wavelength bands, polarization states, phase, etc.) onto each pixel. A fundamental challenge is manipulating the electrical and optical properties at the interface of dissimilar materials. We sought to address the traditional challenges associated with this need via the integration of precisely controlled (semi)metallic nanostructures with III-V semiconductors, using ErAs and related materials as the metals. Our approach began with coupling these metallic nanostructures with growth on patterned templates. We developed a patterning/regrowth process and characterized the deposition of ErAs on a variety of template surfaces using a variety of electrical, optical, structural, and chemically-sensitive techniques. We also examined the optical quality of III-V layers grown above ErAs nanostructures, which is critical for future device applications, and developed a method to achieve optical quality within 80-95% of nominally-identical Er-free structures. These findings led us to invent a technique to grow GaAs that is free of planar defects on full films of ErAs, which is not possible using conventional growth methods. We also extended these studies to other rare earth species.

Distribution Statement

This is block 12 on the SF298 form.

Distribution A - Approved for Public Release

Explanation for Distribution Statement

If this is not approved for public release, please provide a short explanation. E.g., contains proprietary information.

SF298 Form

Please attach your SF298 form. A blank SF298 can be found here. Please do not password protect or secure the PDF The maximum file size for an SF298 is 50MB.

Standard Form 298 FA9550-10-1-0182.pdf

Upload the Report Document. File must be a PDF. Please do not password protect or secure the PDF . The maximum file size for the Report Document is 50MB.

Final Report FA9550-10-1-0182.pdf

Upload a Report Document, if any. The maximum file size for the Report Document is 50MB.

Archival Publications (published) during reporting period:

1. K.W. Park, E.M. Krivoy, H.P. Nair, S.R. Bank, and E.T. Yu, "Cross-sectional scanning thermal microscopy of ErAs/GaAs superlattices grown by molecular beam epitaxy, " Nanotech., vol. 26, pp. 265701-1-5, June 2015.

2. X. Li, V. D. Dasika, P.-C. Li, S.R. Bank, E.T. Yu, "Minimized open-circuit voltage reduction in GaAs/InGaAs quantum well solar cells with bandgap-engineered graded quantum well depths, " Appl. Phys. Lett., vol. 105, no. 12, pp. 123906, Sept. 2014.

3. E.M. Krivoy, S. Rahimi, H.P. Nair, R. Salas, S.J. Maddox, D.J. Ironside, Y. Jiang, G. Kelp, G. Shvets, D. Akinwande, and S.R. Bank, "Growth and characterization of single crystal rocksalt LaAs using LuAs barrier layers," Appl. Phys. Lett., vol. 101, no. 22, pp. 221908, Nov. 2012.

4. K.W. Park, V.D. Dasika, H.P. Nair, A.M. Crook, S.R. Bank, and E.T. Yu, "Conductivity and structure of ErAs nanoparticles embedded in GaAs pn junctions analyzed via conductive atomic force microscopy," Appl. Phys. Lett., vol. 100, no. 23, pp. 233117, June 2012.

5. E.M. Krivoy, H.P. Nair, A.M. Crook, S. Rahimi, S.J. Maddox, R. Salas, D.A. Ferrer, V.D. Dasika, D. Akinwande, and S.R. Bank, "Growth and characterization of LuAs films and nanostructures," Appl. Phys. Lett., vol. 101, no. 14, pp. 141910, Oct. 2012.

6. K.W. Park, H.P. Nair, A.M. Crook, S.R. Bank, and E.T. Yu, "Scanning capacitance microscopy of ErAs nanoparticles embedded in GaAs pn junctions," Appl. Phys. Lett., vol. 99, pp. 133114, Sept. 2011.

7. A.M. Crook, H.P. Nair, D.A. Ferrer, and S.R. Bank, "Suppression of planar defects in the molecular beam epitaxy of GaAs/ErAs/GaAs heterostructures," Appl. Phys. Lett., vol. 99, pp. 072120, Aug. 2011.

8. A.M. Crook, H.P. Nair, and S.R. Bank, "Surface segregation effects of erbium in GaAs growth and their implications for optical devices containing ErAs nanostructures," Appl. Phys. Lett., vol. 98, no. 12, pp. 121108, Apr. 2011.

2. New discoveries, inventions, or patent disclosures:

Do you have any discoveries, inventions, or patent disclosures to report for this period?

No

Please describe and include any notable dates

Do you plan to pursue a claim for personal or organizational intellectual property?

Changes in research objectives (if any):

None

Change in AFOSR Program Manager, if any:

Changed from Dr. Kitt Reinhardt to Dr. Jim Hwang to Dr. Ken Goretta

Extensions granted or milestones slipped, if any:

No cost extension to 04/30/2016 to compensate for Sequestration.

AFOSR LRIR Number

LRIR Title

Reporting Period

Laboratory Task Manager

Program Officer

Research Objectives

Technical Summary

Funding Summary by Cost Category (by FY, $K)

	Starting FY	FY+1	FY+2
Salary			
Equipment/Facilities			
Supplies			
Total			

Report Document

Report Document - Text Analysis

Report Document - Text Analysis

Appendix Documents

2. Thank You

E-mail user

Jul 31, 2016 12:31:25 Success: Email Sent to: sbank@ece.utexas.edu